J Nanopart Res (2019) 21: 72
https://doi.org/10.1007/s11051-019-4513-6

RESEARCH PAPER

Molecular dynamic simulations of ether-coated aluminum nano-particles as a novel hydrogen source

Ruochen Sun · Pingan Liu · Hui Qi · Junpeng Liu · Tao Ding

Received: 20 January 2019 / Accepted: 18 March 2019 / Published online: 30 March 2019

Abstract Aluminum (Al) nano-particles (ANPs) are considered as efficient and well-performed hydrogen source for generation. In this investigation, the ReaxFF molecular dynamic (MD) simulations are employed to uncover the potential of ether-coated ANPs (ECANPs) as a novel hydrogen source. In the very beginning, seven different chemical systems are built as basal datafile and their differences relate to the setting of metal sphere, ether, or water molecules. Those obtained results suggest that the Al cluster has qualified metal–water reaction behavior through strong water adsorption ability at room or much higher temperature. When pure Al cluster is placed under ether solution environment, ether molecules could effectively form a coating layer on Al surface. The removal of surrounding ether agglomerate may lead a little desorption but will not destroy the overall coating configuration. Furthermore, the formation of ether coating could serve as a catalyst and even encourage the water dissociation due to hydrogen bonds. Finally, the storage of powders is assessed through oxidation resistance, showing that the ether coating can protect Al cluster from deep oxidation. With much thinner oxidized layer, the activity of ECANPs could be kept higher than 80% for more than a month.

Keywords Hydrogen · Aluminum · Ether · ReaxFF force field · Modeling · Simulation

R. Sun · P. Liu (✉) · H. Qi · J. Liu · T. Ding
College of Aerospace and Civil Engineering, Harbin Engineering University, Nangang District, Harbin City, Heilongjiang Province, China
e-mail: liupingan631@163.com

R. Sun
e-mail: sunrc836@hotmail.com

H. Qi
e-mail: qihui205@sina.com

J. Liu
e-mail: pureindigo@hrbeu.edu.cn

T. Ding
e-mail: hlgdt2011@163.com

Introduction

Hydrogen gas is a kind of sustainable and eco-friendly fuel with numerous economic, environmental, and social potentials, such as power supply systems in the Arctic zone (Dudoladov et al. 2016). It could effectively bring the improvement in the air environment and slowdown fossil fuel consumption (Mohammadi 2018). So, it is generally believed that hydrogen fuel will meet global energy demand and will eventually be used instead of fossil fuels (Lattin and Utgikar 2007). In contrast to conventional fossil fuels, natural hydrogen fuel is scarce on earth, although the element of hydrogen is the most abundant one in the universe (Russo et al. 2011). Therefore, it becomes necessary to develop the hydrogenation industry for increasing requirements.

Currently, there are four main methods of producing hydrogen gas, and one of them is water electrolysis method. It is said that this method is based on the

dissociation of water into hydrogen and oxygen under the condition of direct current. Available systems for water electrolysis include solid oxide water electrolysis (SOE), alkaline water electrolysis (AWE), alkaline anion exchange membranes (AEMs), and proton-exchange membranes (PEMs) (Chi and Yu 2018). The second method is through the use of biomass. As reviewed by Mudhoo et al., it generally occurs through fermentative reactions and has such advantages as limited pollution and waste management (Mudhoo et al. 2018). Another hydrogenation method is fossil fuel method, which is also reported as the method majorly employed in the industry, due to the characteristic of low-cost and large-scale production (Russo et al. 2011). The final method for hydrogenation is achieved through the reactions of active metal with water. The main advantage of this reaction is that it makes the production of on-demand hydrogen gas possible, thereby solving the challenge of hydrogen fuel storage (Wang et al. 2009).

In terms of the metal–water reaction for hydrogenation, potential alternative metals include zinc (Zn) (Wegner et al. 2006), magnesium (Mg) (Grosjean et al. 2006), and Al (Shmelev et al. 2016). As one of the most plentiful crystal metal elements on earth, this study investigates an Al-based material as a novel hydrogen source. It is reviewed by H.Z. Wang et al. where they find that active Al and its alloys are qualified for hydrogenation by reactions with water or even hydrocarbons, and reactive conditions like alkaline and neutral are both feasible for Al–water reaction systems (Wang et al. 2009). Due to the oxidation on the Al surface, several active methods are investigated on Al as well (Ilyukhina et al. 2017, Liu et al. 2018a, b, Fan et al. 2010, Shmelev et al. 2016).

With the consideration of reactant size, it seems that nano-sized Al powder may provide better performances relate to hydrogenation. General structure properties of metal clusters have been studied and reviewed previously (Baletto and Ferrando 2002, 2005). As a typical energetic carrier, Al nano-particles are widely applied to explosives, pyrotechnics, and propellants (Gromov et al. 2014, Dreizin 2009, Meda et al. 2007). It is also believed that Al nano-particles (ANPs) have the potential to undergo rapid hydrogenation (Shimojo et al. 2010). But, the high surface-to-volume ratio also brings challenges of oxidation and further affects its activity negatively (Guo et al. 2008). Thus, the surface passivation operation becomes necessary for ANPs. As a nano-scaled energic material, ANPs must be passivated for higher hydrogenation performance. In the past, many studies have focused on Al surface passivation by 360° coating. Their passivation effect and performance are diverse depending on coating material and technology. The passivating layer should not only keep coated in air, but also be prone to be destroyed under liquid water. So, organic coatings are under great concern (Liangui Guo et al. 2008). Previously, some organic coatings like 1,2-epoxyhexane (Jelliss et al. 2013), polytetrafluoroethylene (Kim et al. 2016), and PMMA (Liu et al. 2007) have been investigated. The organic material applied in this study is ether. Because it is light and slightly soluble, those desorbed liquid ether molecules will form a thin organic layer on water, which will not affect the Al–water reactions.

Method and setup

ReaxFF-based molecular dynamic simulations

Compared with first-principal calculations, MD simulations serve as an effective method for atomistic scale investigations, which generally combines physics, chemistry, and computing science based on Newton mechanics. In the framework of the MD simulations, ReaxFF force field is a powerful instrument for reactive heterogeneous systems. Essentially, the training of ReaxFF force field mainly relies on quantum mechanics and experiments. Other than conventional force fields, ReaxFF enables the description of bond breaking/formation and charge transfer (Wang et al. 2015). Whether a chemical bond is broken or not is determined by "bond order" (Liu and Guo 2017, Tersoff 1986). According to each step of MD result, such as interatomic distance, bond orders for each pair of atoms could be obtained. In this study, three different ReaxFF files are adopted. The first ReaxFF file was coded by Hong and Duin (2016), through which, reaction behaviors among Al, carbon (C), hydrogen (H), and oxygen (O) are defined. Relative surface investigations for ANPs are also progressed by their contribution (Hong and Duin 2015, Zhang et al. 2018), while another specified ReaxFF was developed by Van Duin et al. (2010) and is validated for copper (Cu)/water/oxide interactions. In the case of Cu cation/water system, it successfully described the interaction process. The final ReaxFF was developed by Aryanpour et al. (2010), whose initial

model is designed for α-FeOOH (goethite)–water interactions; hence, the iron–water system is fitted for this situation as well. Equation 1 shows the expression of the total energy of the system by ReaxFF force field (Hong and Duin 2015).

$$E_{\text{system}} = E_{\text{bond}} + E_{\text{over}} + E_{\text{under}} + E_{\text{lp}} + E_{\text{val}} + E_{\text{tors}} + E_{\text{vdWaals}} + E_{\text{Coulomb}} \quad (1)$$

where E_{system} is the total energy, E_{bond} is the bond energy, E_{over} is the overcoordination energy, E_{under} is the undercoordination energy, E_{lp} is the lone-pair energy, E_{val} is the valence angle energy, E_{tors} is the torsion angle energy, E_{vdWaals} is the van der Waals energy, and E_{coulomb} is the coulomb energy. Each MD simulation in this research is conducted on the platform of Large-scale Atomic/Molecular Massively Parallel Simulator (LAMMPS) which is freely available online. The export of LAMMPS datafile is achieved by the visual molecular dynamics (VMD) (William Humphrey et al. 1996). As for the choice of time step, both 0.2 fs and 0.5 fs have been applied previously on similar models (Liu et al. 2019a, b, Yi Ran Zhang et al. 2018). Thus, an extra simulation has been performed to validate if the lower time step can bring some positive effects. For those works in "Reactive behaviors of metal clusters with water molecules" section, it is obtained that there is no explicit difference on results from these two time steps. Due to the consideration of computing efficiency, the length of each time step is assigned as 0.5 fs. As MD simulations in this study are described as a function of the temperature, it is reasonable to control the temperature of each molecule. Based on Nose/Hoover thermostat (Hoover 1984; Nosé 1984), all of the following MD simulations (except annealing process) are run within canonical ensemble (NVT) for 2×10^5 iterations (100 ps). Because of the effective reacting and coating behaviors, it has been validated that the time scale is enough for the study, and further simulations will be in equilibrium and unnecessary to be presented.

As the object of this study is Al nano-particles, an Al cluster containing 2015 atoms is created by LAMMPS using FCC crystal style and its radius is 2 nm. Initially, the cluster is built around a bulk center; thus, it is shown as an ideal sphere. In this occasion, some edge effects are not beneficial for the simulations result; therefore, the Al cluster should be annealed before hydrogenation reactions (Russo et al. 2011). The annealing simulation is integrated by micro-canonical ensemble (NVE), and the temperature is controlled by Berendsen et al. (1984) theory with damping constant of 100 fs. The energy of system is conserved at the beginning; then, overall heating and cooling processes last for approximately 1500 ps. The heating process is progressed lineally at the rate of 6 K/ps and stopped when the temperature reached 1200 K. Atoms in the Al cluster are fully rearranged at this peak temperature because it has already been higher than Al melting temperature (933 K). Then, the cooling process is processed at two stages. In the first stage, the Al cluster is cooled rapidly for about 400 K, which is for the solidification effect while atoms have already been fully rearranged. Afterwards, temperature changes are on gradient in the second stage, ensuring the minimum potential energy of the obtained Al cluster. The overall heating and cooling processes are demonstrated in Fig. 1. Due to the computing requirement in this study, annealed Cu and iron (Fe) clusters are also prepared in the similar mode, and their differences lie in peak and solidification temperatures. Next, those prepared metal clusters are all placed in the 3-dimentional center of a $9 \times 9 \times 9$ nm cubic simulation box with periodic boundaries.

For the evaluations of metal–water reactions, metal coating and oxidation resistance, molecules such as water, oxygen, and ether are placed randomly in the vacuum of box. The placement of those nonmetal molecules is determined by Packmol, which is a freely available program for packing optimization (Martínez et al. 2009). All configurations in this study are obtained using OVITO (Stukowski 2010). Different simulation systems containing metal cluster and nonmetal molecules are summarized in Table 1. In which, systems $1^{\#}$ to $3^{\#}$ are designed to compare hydrogenation performances of Al, Cu, and Fe metal clusters. As for temperature, metal clusters are fixed at 0 K while water molecules are fixed at approximately 1600 K to achieve higher reacting rate (Russo et al. 2011), and water molecules in this temperature are gaseous with low density. It is concluded in previous investigations that either too few or too many water molecules may restrain hydrogenation simulations (Shimojo et al. 2010, Russo et al. 2011). Therefore, 200 water molecules are assigned in the system. Next, systems $4^{\#}$ and $5^{\#}$ are used to prepare ether-coated Al nano-particle and further test its hydrogenation behaviors. The temperature of ether is fixed at 800 K due to the consideration of coating effect (Liu et al. 2018b). On this occasion, 1500 ether molecules are

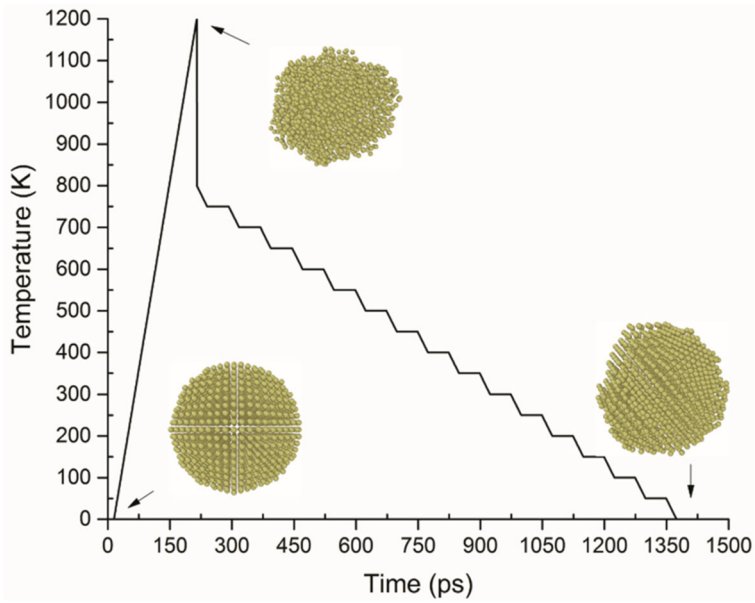

Fig. 1 Annealing process of Al cluster in simulation box

placed in the vacuum, which is about half of its real bulk density, and it has been validated that this density is approximate for coating in such high temperature. Besides, the number of 211 ether molecules is obtained by computing results discussed in "Mechanism of coating ether molecules on ANP surface" section; then, the setting of water is same with former systems. Finally, there are 340 oxygen gas molecules placed in systems $6^{\#}$ and $7^{\#}$. As the real density of oxygen gas is too low to satisfy the MD simulation, the quantity of oxygen molecules is increased to be about 30 times higher than reality, while this part of simulation is performed at room temperature.

Experimental methods

Gas capacity method

Gas capacity method is a reliable approach for estimating the hydrogen generation by metal–water reactions, which could measure the total volume of hydrogen gas and then further evaluate the activity of metal powders (Eq. 2). The initial materials of this experiment mainly fall into two categories: metal powders (about 0.1–0.3 g) and NaOH solution (8 g/L, 150 mL) (Wang et al. 2009). There are four kinds of metal powders that have been prepared including Al micro-particles, Cu micro-particles, Fe micro-particles, and ether-coated ANPs (ECANPs). The application of micro-particles is mainly due to the consideration of experimental cost and corrosion effect. Ether-coated Al particles have been tested in nano-size for the accuracy of hydrogenation result, because it is the critical object in this study. The hydrogen generator is a glass flask, which is attached to a deionized water tank and a tube with volume scales. A pre-test has been progressed to test its sealing property and air ejection by hydrogen gas. Additionally, a thermometer is inserted into the tank for recording environmental temperature.

$$C_{\mathrm{Al}}(\mathrm{wt.}\%) = \frac{V_{\mathrm{H_2}} \times \rho_{\mathrm{H_2}} \times 2 \times M_{\mathrm{Al}}}{m \times 3 \times M_{\mathrm{H_2}}} \times 100\% \qquad (2)$$

where C_{Al} is the percentage of active Al (%), V_{H2} is the volume of H_2 (L), ρH_2 is the density of H_2 (g/L), M_{Al} is the molecular weight of Al (g/mol), M_{H2} is the molecular weight of H_2 (g/mol), and m is the mass of specimen (g).

Other experiments

Transmission electron microscope (TEM) testing technique generally allows researchers to observe the microstructure with high resolution (Yano et al. 2018). In this study, the final effect of ether-coated ANPs is evaluated by TEM (Hitachi Limited H-7650) to confirm the appearance of coated layer and it is also utilized for validating the MD simulation result. The acetone dispersion

Table 1 The various chemical systems for MD simulations

System number	Metal cluster	Addition 1	Number of addition 1	Addition 2	Number of addition 2
1#	Al	Water	200	Null	0
2#	Cu	Water	200	Null	0
3#	Fe	Water	200	Null	0
4#	Al	Ether	1500	Null	0
5#	Al	Ether coating	211	Water	200
6#	Al	Ether coating	211	Oxygen gas	340
7#	Al	Oxygen gas	340	Null	0

is used in specimen and the accelerating voltage is about 300 kV.

Thermogravimetric analysis (TGA) is a precise method of estimating the property of oxidation resistance for ECANPs, because a qualified energetic carrier should maintain high activity under a certain life cycle. In this study, TGA tests are performed using PerkinElmer Pyris 6 TGA analyzer under the condition of natural air environment. When powders around 0.5 mg are placed in the ceramic crucible, the mass of the powders is then detected as the function of time and temperature. The temperatures ranging from 308 to 573 K with a heating rate of about 10 K/min are preset for TGA analyzer.

Oxidation–reduction titration (ORT) could generally provide the activity of ECANPs by a series of reactions; thus, it works as the validation for gas capacity method in this investigation. Initially, ECANPs react with ethanol–$FeCl_3$ solution in a specified blender for 30 min, which could release an amount of Fe^{2+} ions. To eliminate Fe^{3+} ions, the dilute phosphoric acid solution is then titrated until the solution is achromous. Finally, the titration solution turns to permanganate solution (0.02 mol/L). The whole titration stops while the whole solution begins to become purple. By recoding how many permanganate solutions have been utilized, the percentage of active Al could be further calculated. Equation 3 is the function of the permanganate solution and active Al.

$$C_{\mathrm{Al}}(wt.\%) = \frac{C_{\mathrm{KMnO_4}} \times V_{\mathrm{KMnO_4}} \times M_{\mathrm{Al}} \times 5}{M_{\mathrm{KMnO_4}} \times m \times 3} \times 100\% \quad (3)$$

where C_{Al} is the percentage of active Al (%), C_{KMnO4} is the concentration of $KMnO_4$ solution (mol/L), V_{KMnO4} is the volume of $KMnO_4$ solution (L), M_{Al} is the molecular weight of Al (g/mol), M_{KMnO4} is the molecular weight of $KMnO_4$ (g/mol), and m is the mass of specimen (g).

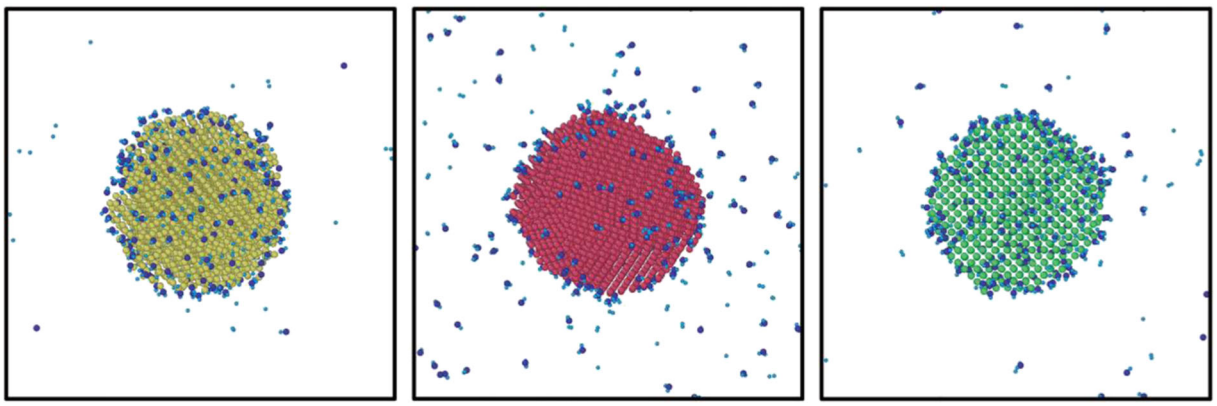

Fig. 2 Images of Al (1#), Cu (2#), and Fe (3#) system configurations

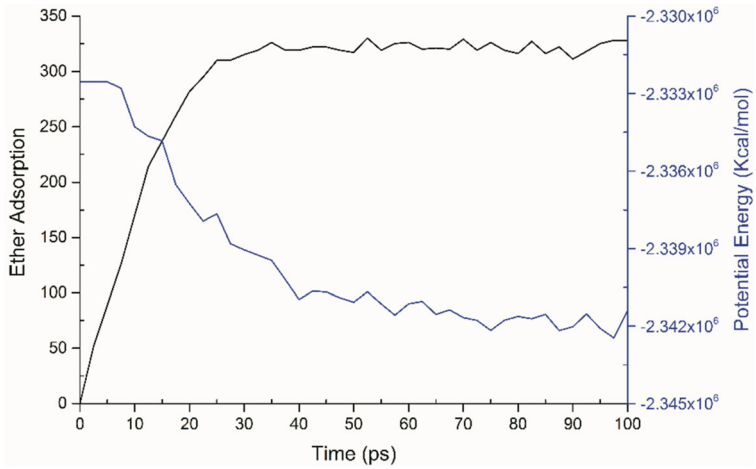

Fig. 3 The number of adsorbed ether molecules and change in potential energy as a function of time

Results and discussions

Reactive behaviors of metal clusters with water molecules

Overall, it is essential to validate that the Al powder is a better choice compared with other familiar metal powders. With the platform of MD simulations, systems $1^{\#}$, $2^{\#}$, and $3^{\#}$ are studied in this section. A qualitative view of Fe-, Al-, and Cu-based MD systems after 100 ps are illustrated in Fig. 2.

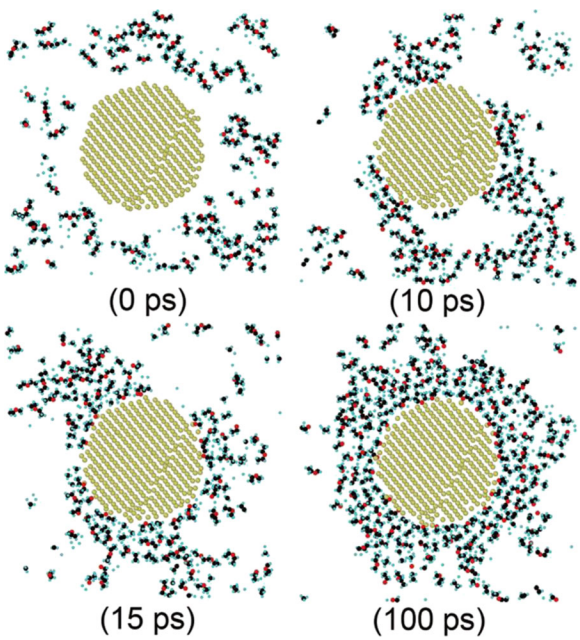

Fig. 4 Snapshots of cross section of system $4^{\#}$ configuration

As shown in Fig. 2, almost all water molecules have reacted with Al or Fe cluster after 100 ps and released a lot of hydrogen atoms. However, this phenomenon is contrary to the Cu cluster as there are few adsorbed water molecules on its surface. The dissociation of water molecules on metal surface is not completed by themselves, but by the help of the surrounding intact water molecules (Shimojo et al. 2010). According to the Grotthus mechanism (Yoshida and Tokumasu 2010), the dissociation of water molecules into OH^- and H^+ starts from protons disassociating from water molecule and then transferring by hopping the network of hydrogen bonds. In this process, hydrogen bonds are provided by surrounding intact water molecules, wherein the activation barrier for this dissociation mechanism is much lower as compared with the self-produced ones (Shimojo et al. 2010). In addition to the Grotthus mechanism, the number of water molecules is critical for the metal–water reaction. The dissociation behavior is affected when the surface coverage of cluster reaches a maximum state or when surrounding water molecules are not adequate for assistance (Russo et al. 2011). In this study, the stability of Cu cluster is presented as the weak adsorption behavior. From the onset to end, there are still a lot of free water molecules in the box. On the contrary, the free water molecules could be captured rapidly by Al and Fe clusters under similar conditions. It is observable that these adsorbed water molecules in system $2^{\#}$ are not adequate to activate Grotthus mechanism and release hydrogen atoms further.

For systems $1^{\#}$ and $3^{\#}$, it does not mean that both Al and Fe clusters are suitable for hydrogenation. As mentioned before, these simulations are processed at

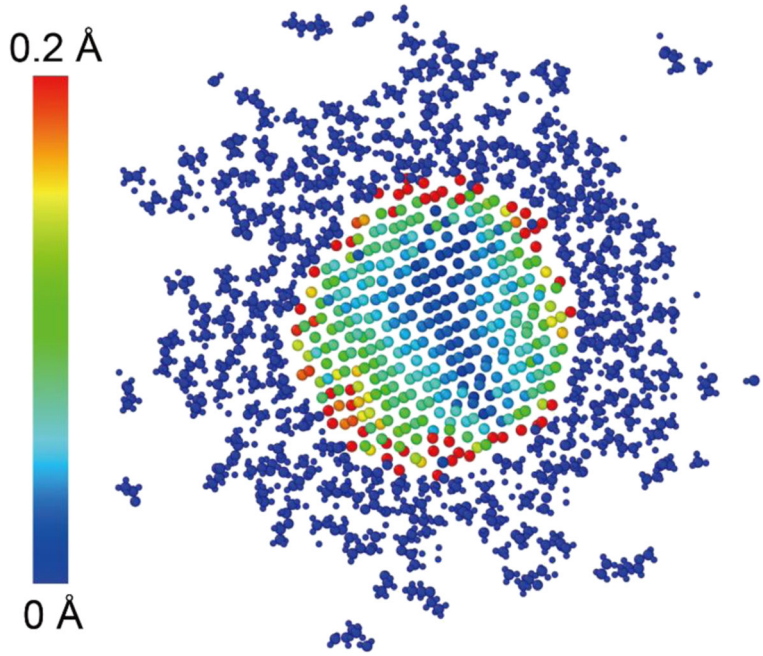

Fig. 5 Snapshot of cross section of Al atom displacement at 100 ps

1600 K. Therefore, those water molecules are vapor while corresponding to experimental conditions. It is well known that Al could react with water in the alkaline environment at room temperature (H.Z. Wang et al. 2009). At the same time, a similar reaction for Fe must be under a high temperature of up to 840 K (Budiman et al. 2016). In other words, Fe powder may have the potential to be a hydrogen source. However, it will not be as economical as Al powder.

Mechanism of coating ether molecules on ANP surface

A molecular dynamic preparation by system 4# is processed to investigate the mechanism of ether coating

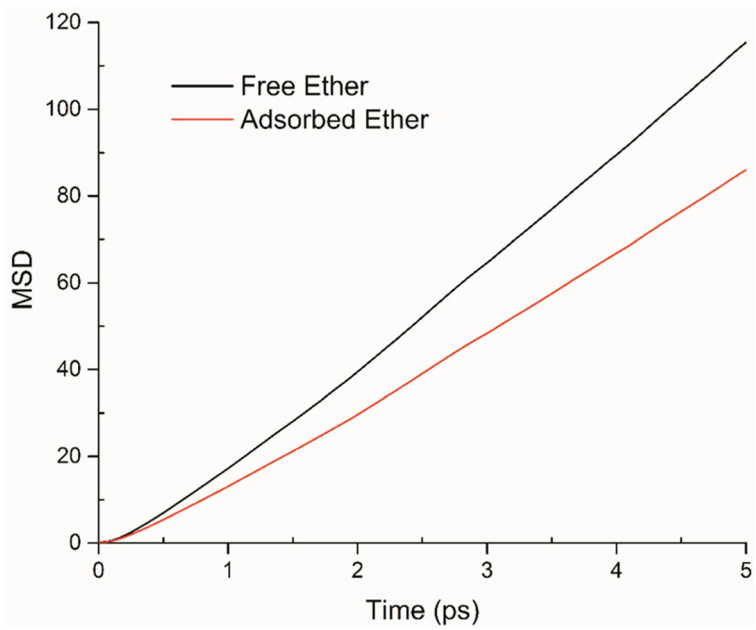

Fig. 6 MSD plot for free and adsorbed ether molecules after coating process

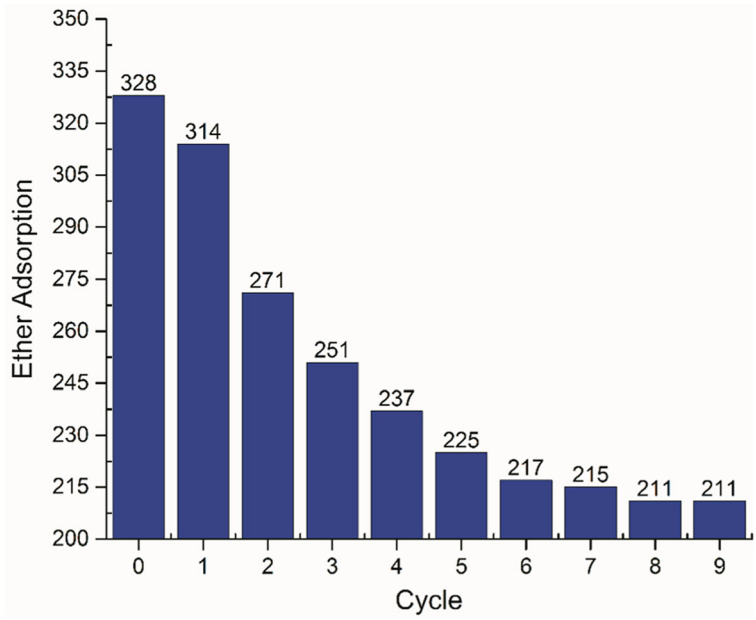

Fig. 7 The number of ether molecules in each deleting cycle

process as well as to pave the way for following discussions in "Effect of ether coating on Al–water reaction" and "Oxidation resistance of ether-coated ANPs." The simulated preparation is divided into two stages. The first stage is based on system $4^{\#}$, and in this stage, the layer of coated ether molecules will be formed on particle surface. In the second stage, a 9-cycle deleting command is induced to delete those free ether molecules. Finally, a stably coated Al cluster is obtained at room temperature.

The overall coating process is illustrated in Fig. 3 by the quantity of adsorbed ether molecules and potential energy. From the figure, the adsorption curve is seen to increase almost linearly in the first 25 ps. From then, the trend stabilizes at around 328 molecules in solution environment. In this occasion, the potential energy of the whole system tends towards stability as well. Figure 4 is the 5-Å-thick cross section of the adsorption system, which includes three linear adsorbing configurations (0–15 ps) as well as a final configuration (100 ps). As well, the formation of coating layer could generally be presented by this figure. Since the bulk density of ether in this simulation is far lower than its

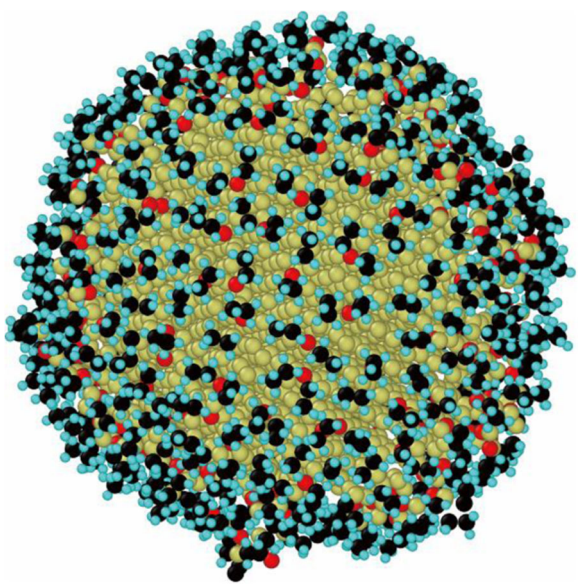

Fig. 8 Obtained configuration of ether-coated Al cluster

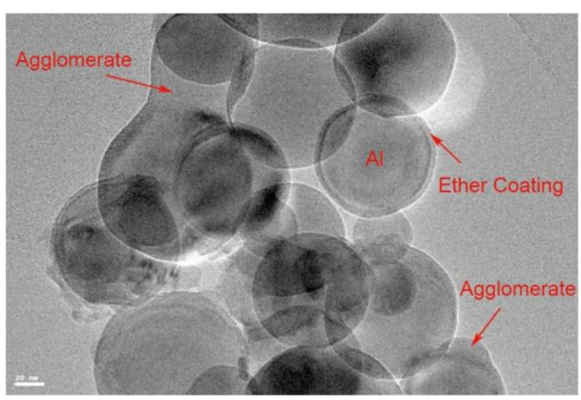

Fig. 9 TEM images of ether-coated Al nano-particles

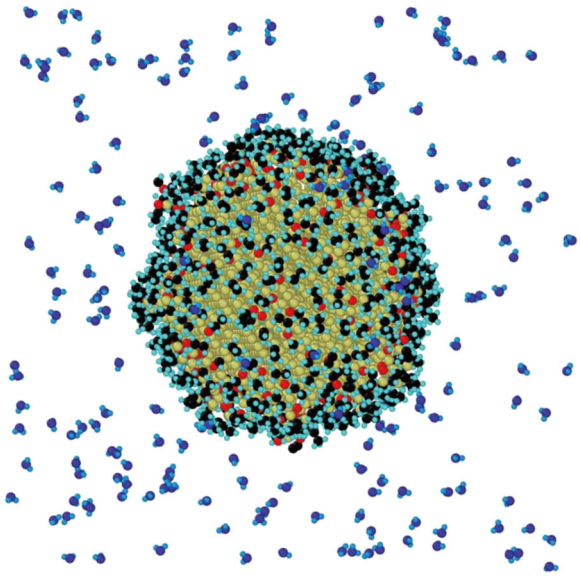

Fig. 10 Initial configuration of system $5^{\#}$

real density, free ether molecules are more likely to be agglomerated, and this agglomerate trend will be around the Al cluster due to the adsorbing effect. The formation of agglomerate exerts pressure to Al cluster as well. Figure 5 is the snapshot of final configuration (100 ps) colored by Al atom displacement. As shown, the outer Al atoms displaced nearly 0.2 Å as a consequence of the pressure effect from ether agglomerate. Although there are many ether molecules nearby, it does not mean that all those ether molecules around have been adsorbed.

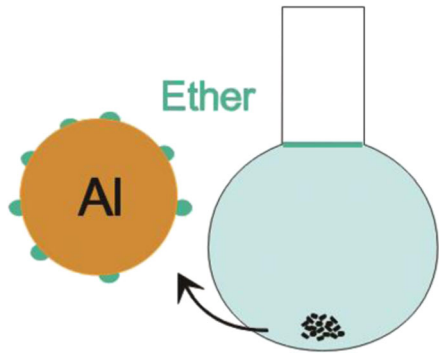

Fig. 12 Schematic diagrams of ECANPs under water

By configured estimation, it is a single-layer adsorption. The mean square displacement (MSD) analysis summarized in Figure 6 is applied to present the difference of free and adsorbed ether molecules. As illustrated, the diffusion movement of free ether molecules is explicitly higher than the adsorbed ones.

To obtain a purely coated Al cluster, it is critical to remove those free ether molecules, which is the requirement in the second stage. As indicated in Fig. 7, the number of adsorbed ether molecules decrease largely from cycle 1 to cycle 9. As mentioned previously, the ether agglomerate exerts much pressure to Al atoms and causes the displacement. To some extent, the coated ether molecules act as the accepter and medium for this pressure. When free ether molecules are removed, their pressure will be released as well. Meanwhile, some of them will be desorbed and returned to be free molecules.

Fig. 11 Water dissociation for systems $1^{\#}$ and $5^{\#}$ as a function of time

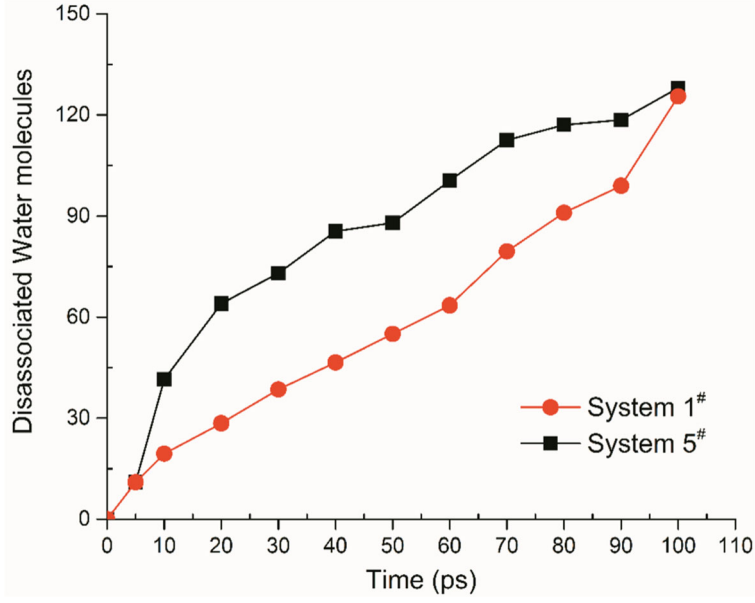

Table 2 Hydrogenation performance of ECANPs

Temperature (°C)	Reactant	Mass (g)	Volume of H_2 (L)	Activity (%)
23	ECANPs	0.1	0.112	90.619
23	ECANPs	0.15	0.176	94.934
23	ECANPs	0.2	0.221	89.406
	Average			91.653

The effect of pressure release gets lower and finally vanishes in cycle 8. As such, the number of adsorbed ether molecules is stable in cycles 8–9, and finally confirmed as 211. The obtained configuration after this 9-cycle deletion is presented in Fig. 8.

Validating the above MD simulation result experimentally confirms the coating effect. Some ECANPs were produced through a physical adsorption method in the laboratory of Harbin Engineering University. Moreover, the TEM result is shown in Fig. 9. It is estimated that the diameters of those particles are around 40–90 nm, and the thickness of ether coating is about 4.6 nm. Similar with MD result, the TEM image also presents the formation of ether agglomerate. In the bottom right corner of the image, there is a single agglomerate on the surface of coated ANPs. In the top left corner of image, a much larger ether agglomerate eventually linked two single ECANPs nearby. Overall, it seems that this result is in line with MD simulations. More quantitative characterizations about the ECANPs have been published (Liu et al. 2019a, b).

Effect of ether coating on Al–water reaction

As a novel hydrogen source, the reaction behavior of ether-coated Al cluster with water molecules is worth studying, because the formation of ether coating should not interfere with the hydrogenation result. For this purpose, system $5^{\#}$ with 200 water molecules is investigated in this section. As a control group in system $1^{\#}$, water and ether molecules in system $5^{\#}$ are also fixed around 1600 K, while the number of environmental water molecules is the same as well. The initial configuration of which is presented as Fig. 10. In system $5^{\#}$, the coated Al cluster is just obtained in "Mechanism of coating ether molecules on ANP surface." Besides, a 5-Å-radius vacuum is set between water solution system and coated cluster.

During the 100 ps length simulation, several ether molecules are desorbed under the pressure of water, and then made the ether featured a catalyst-like effect. As Fig. 11 shows, the number of disassociated water molecules for coated Al cluster is obviously higher than uncoated one, and finally, a similar consequence is

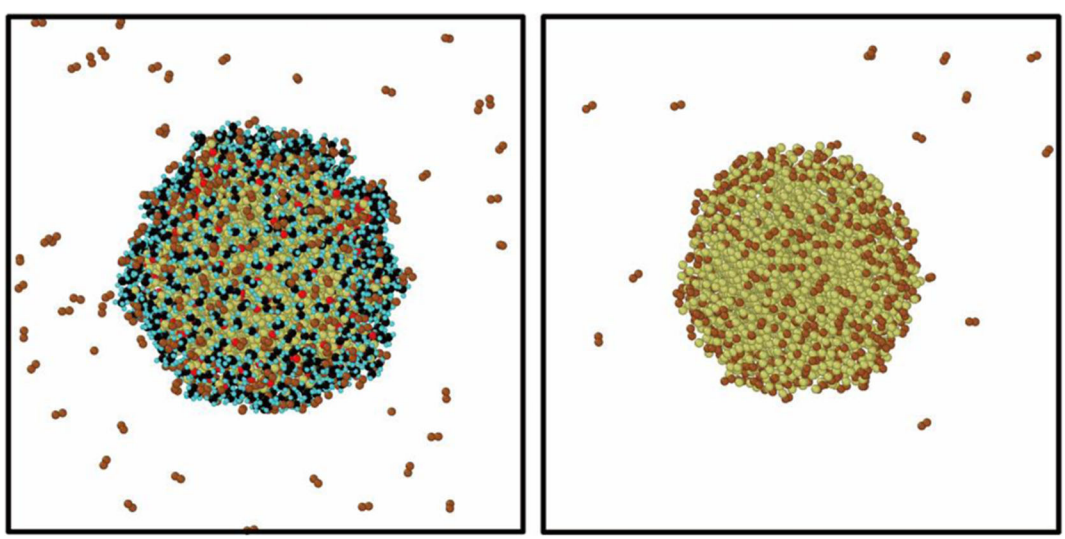

Fig. 13 Final snapshots ($t = 100$ ps) of systems $6^{\#}$ (left) and $7^{\#}$ (right)

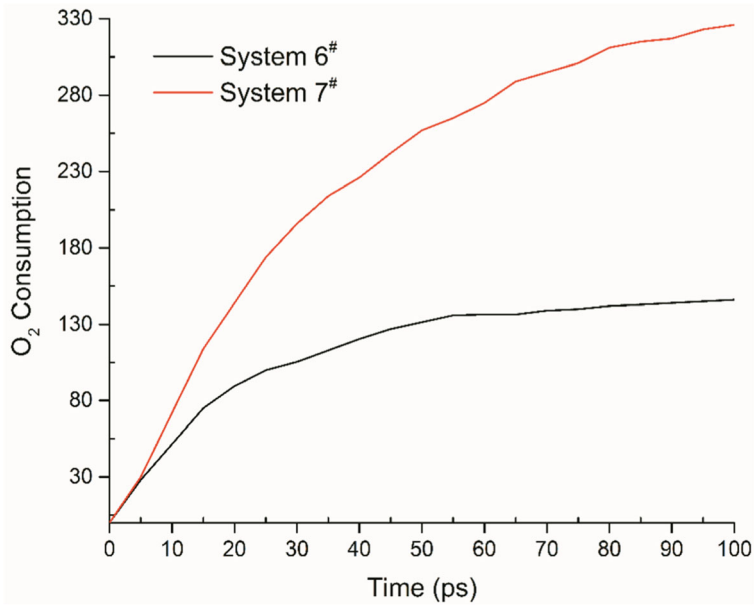

Fig. 14 Number of oxygen gas molecules consumed as a function of time

made. Generally speaking, this is due to the characteristics of ether. Chemically, the ether group could act as a hydrogen-bond accepter (Sawamura et al. 1986), but it is unable to be a donor. As mentioned in "Reactive behaviors of metal clusters with water molecules," the dissociation of water molecules mainly depends on Grotthus mechanism. Therefore, the placement of ether on surface could accelerate the disassociating behavior, which is just like a catalyst.

One limitation of MD simulation in this section is that the pressure of water molecules is impractical to reach realistic level because of limited computing cost. The bulk density of liquid water in real environment is 1 g/cm^3, while the density of water molecules in simulation box is about 0.00901 g/cm^3. It is almost 111 times lower than that of liquid water. Another critical issue is that relevant hydrogenation experiments may induce supersonic vibration for a better performance, but it could not be simulated by MD. Because of these two factors, the large-scale desorption of ether coating under water could not be observed by MD. It is estimated that majority of ether molecules will be desorbed from Al cluster and form an extremely thin layer on water plane (Fig. 12). For validating the realistic hydrogenation performance of ECANPs, three parallel gas capacity method experiments are completed. Relevant results are listed in Table 2. According to the volume of obtained hydrogen gas, it seems that

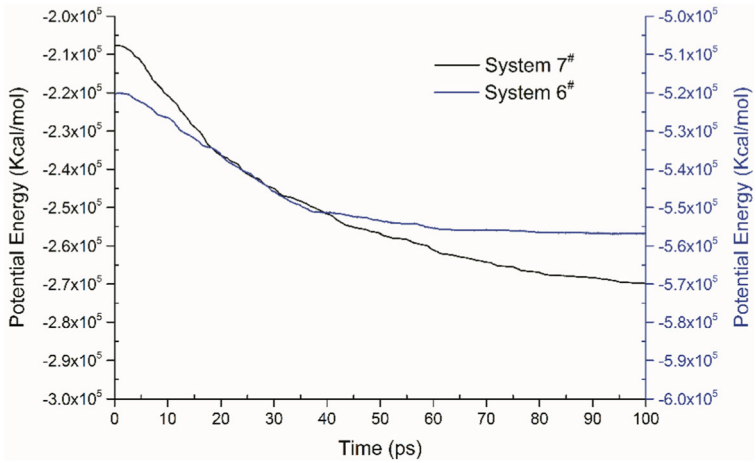

Fig. 15 Decrease in potential energy as a function of time

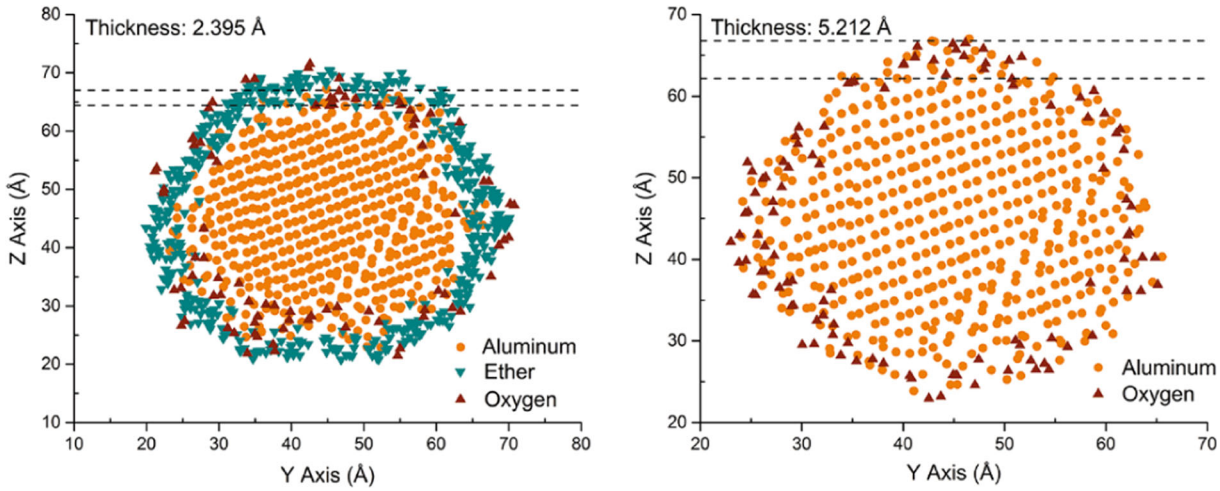

Fig. 16 Scatter plots of cross sections of systems 6# (left) and 7# (right)

ECANPs have qualified performance as a hydrogen source, and there is no negative effect. Based on Eq. 2, the activity of as-produced ECANPs is calculated as 91.653%. Compared with uncoated micro-Al particles (76.865%), this result is more satisfying.

Oxidation resistance of ether-coated ANPs

The storage of hydrogen is a critical barrier for the hydrogen economy and technique, but currently, available methods are still unable to meet all requirements for hydrogen applications (Mohammadi 2018). In this study, the challenge of hydrogen storage is transferred to that of ECANP energetic material. For keeping high activities during the storage, the ECANPs should have qualified oxidation resistance performance. With the help of MD simulations, systems 6# and 7# with 340 oxygen gas molecules in each system are investigated in this section. The final snapshots (100 ps) of ether-coated Al cluster (system 6#) and uncoated Al cluster (system 7#) are presented in Fig. 13. Through this comparison, the differences on oxidation resistance are shown explicitly, as there are much more free oxygen gas molecules in the system of ether-coated Al cluster. Statistically, there are 14 free O_2 molecules in system 7#, while the number for system 6# is more than 3 times larger than that of previous one. To some extent, free O_2 molecules are nearly isolated by the appearance of

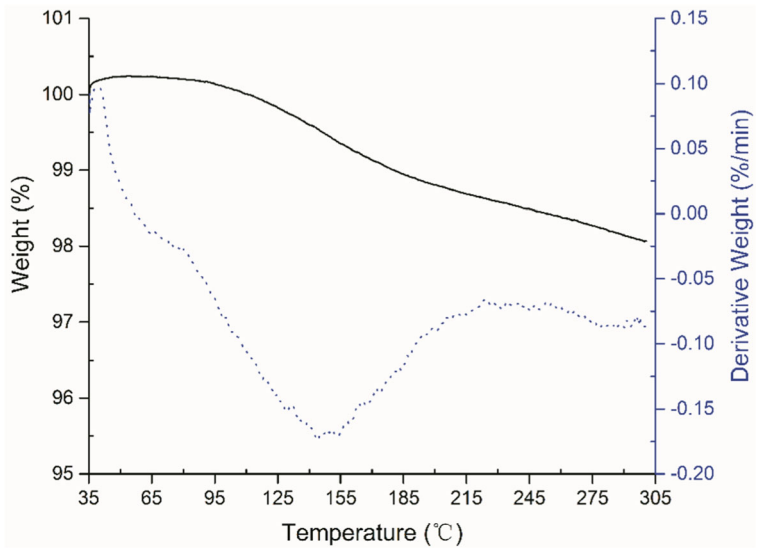

Fig. 17 TG-DTG plot for ECANPs

Table 3 Activities of ECANPs in different days tested by gas capacity method (method 1) and oxidation–reduction titration (method 2) at 20–23 °C

Dates	Volume of H_2 (L)	Activity by method 1 (%)	Volume of $KMnO_4$ (L)	Activity by method 2 (%)
1	See Table 2		0.194	92.089
10	0.311	83.877	0.181	85.918
20	0.302	81.449	0.174	82.595
30	0.298	80.371	0.171	81.171

ether-coating layer; therefore, this is so called oxidation resistance for ANPs.

For exploring this oxidation resistance phenomenon in more detail, the amount of consumed oxygen gas molecules in two systems as a function of time is plotted in Fig. 14. In this statistic, the number for system $6^{\#}$ is only accounted by those oxygen atoms that are inside the Al cluster. This is because there are also many oxygen atoms that are adsorbed on the surface of ether-coating layer. They are neither free oxygen atoms, nor reacted oxygen atoms. Accurately, they belong to physical adsorbed oxygen atoms, so it is unexpected to account them as consumptions. Comparing with system $7^{\#}$, the number of consumed oxygen molecules for system $6^{\#}$ is nearly half of previous one. In other words, the appearance of ether-coating layer doubles the oxidation resistance of Al cluster. Further, this result is validated in Fig. 15. The deviation of initial and final value shows that the reaction in system $6^{\#}$ is as much as half of system $7^{\#}$ by recording the potential energy of each system as a function of time. The ability oxidation resistance could also be presented on the thickness of alumina. As Fig. 16 shows, the thickness of alumina in the cross section of ether-coated Al cluster is about 2.395 Å. While the alumina layer of uncoated Al cluster is as thick as 5.212 Å.

Although MD simulations result shows a good oxidation resistance for ether-coated Al cluster, it is still worthwhile to validate this property by experiment and further investigate its temperature dependence. So, a TGA experiment is carried out for this purpose with a temperature range from 35 to 300 (°C). Similar with MD simulations, the ether coating layer could not completely cover the ANPs; thus, a little oxidation happens around 65 (°C) in Fig. 17. After that, the weight decreases due to the volatilization of organic solvent (agglomerate) or moisture on the surface of ECANPs. Generally, the TGA experiment shows a satisfying oxidation resistance for ECANPs from 35 to 300 °C. Another typical factor for oxidation resistance is the date dependence, so the ECANP specimen with each weighed 0.3 g were stored in natural environment for 10, 20, and 30 days, respectively. Activities of these powders are experimented by gas capacity method and oxidation–reduction titration for validation. As Table 3 shows, activities of newly produced ECANPs are more than 90%, but it will decrease largely in the first 10 days. Finally, activities of ECANPs could keep higher than 80% within a month. So, the potential of these ECANPs is largely illustrated by these activity results, as a high activity will lead a high hydrogen energy density.

Conclusion

Depending on MD simulations and ReaxFF force field, advantages of ether-coated Al cluster as a novel hydrogen source have been investigated. Experiments, such as TEM, gas capacity method, and TGA and ORT have been processed for validation. Initially, excellent reactive performance of Al is illustrated through comparisons with Fe and Cu. According to Grotthus mechanism, the reactive activity of Al and Fe at high temperature is due to strong water adsorption ability. The number of adsorbed water could quickly reach a suitable value and encourage its dissociation. However, this behavior for Cu is explicitly weaker than Fe and Al. Based on experimental result, Al powder could keep this performance while at room temperature, while Fe could not. Therefore, it is reasonable to choose Al-based nanomaterials for hydrogenation.

Additionally, the formation of an ether coating layer on Al cluster surface is also studied. This simulation not only studied the coating behavior but also paved the way for following assessments. It seems that Al cluster could be effectively coated under ether solution environment,

finally reaching a nearly stable state. Due to ether agglomerate nearby, outer Al atoms could be displaced up to 0.2 Å. When these free ether molecules are removed, the pressure for coated ether and Al cluster will be released. Subsequently, some adsorbed ether molecules will be desorbed. The final adsorption configuration still shows a well-coated Al cluster. This configuration is validated by TEM image of self-produced ECANPs.

Based on ether-coated Al cluster, the reactive performance with water is studied. Due to ether catalyst effect, it appears that the reacting speed of coated Al cluster with water is higher than before. In terms of catalyst effect, this is because ether group could act as a hydrogen bond accepter and further encourage the dissociation of adsorbed water molecules. Experimentally, the hydrogen performance of ECANPs is even better than Al micro-particles by higher activity. As a result, the property of oxidation resistance is finally examined. It demonstrates that the appearance of ether coating could effectively resist the oxidation reaction. The performance of oxidation is not only shown by oxygen consumption, but also is presented by oxidized configuration. By assessments of cross section, it seems that oxygen atoms are just on ether-coating surface, but is not reacted with Al. The thickness of oxygen layer for uncoated Al cluster is about 5.212 Å, while it is only 2.395 Å for ether-coated one. Finally, the oxidation resistance of real ECANPs is validated by TG-DTG plot. Moreover, activity tests also show that the storage cycle for those produced ECANPs is no less than a month.

Funding information This investigation is supported by The Fundamental Research Funds for Central Universities (HEUCFG201815).

Compliance with ethical standards

Conflict of interest The authors declare that they have no conflict of interest.

References

Aryanpour M, van Duin ACT, Kubicki JD (2010) Development of a reactive force field for iron-oxyhydroxide systems. J Phys Chem A 114:6298–6307

Baletto F, Ferrando R (2002) Crossover among structural motifs in transition and noble-metal clusters. J Chem Phys 116:3856–3863

Baletto F, Ferrando R (2005) Structural properties of nanoclusters: energetic, thermodynamic, and kinetic effects. Rev Mod Phys 77:371–423

Berendsen HJC, Postma JPM, van Gunsteren WF, DiNola A, Haak JR (1984) Molecular dynamics with coupling to an external bath. J Chem Phys 81:3684–3690

Budiman F, Bashirom N, Tan WK, Razak KA, Matsuda A, Lockman Z (2016) Rapid nanosheets and nanowires formation by thermal oxidation of iron in water vapour and their applications as Cr (VI) adsorbent. Appl Surf Sci 380:172–177

Chi J, Yu H (2018) Water electrolysis based on renewable energy for hydrogen production. Chin J Catal 39:390–394

Dreizin EL (2009) Metal-based reactive nanomaterials. Prog Energy Combust Sci 35:141–167

Dudoladov AO, Buryakovskaya OA, Vlaskin MS, Zhuk AZ, Shkolnikov EI (2016) Generation of hydrogen by aluminium oxidation in aquaeous solutions at low temperatures. Int J Hydrog Energy 41:2230–2237

Fan M-q, Sun L-x, Xu F (2010) Experiment assessment of hydrogen production from activated aluminum alloys in portable generator for fuel cell applications. Energy 35:2922–2926

Gromov A, DeLuca LT, Il'in AP, Teipel U, Petrova A, Prokopiev D (2014) Nanometals in energetic systems: achievements and future. Int J Energetic Materi Chem Propulsion 13:399–419

Grosjean M-H, Zidoune M, Roué J-YHL (2006) Hydrogen production via hydrolysis reaction from ball-milled Mg-based materials. Int J Hydrog Energy 31:109–119

Guo L, Song W, Hu M, Xie C, Chen X (2008) Preparation and reactivity of aluminum nanopowders coated by hydroxyl-terminated polybutadiene (HTPB). Appl Surf Sci 254:2413–2417

Hong S, Duin ACT v (2015) Molecular dynamics simulations of the oxidation of aluminum nanoparticles using the ReaxFF reactive force field. J Phys Chem C 119:17876–17886

Hong S, Duin ACT v (2016) Atomistic-scale analysis of carbon coating and its effect on the oxidation of aluminum nanoparticles by ReaxFF-molecular dynamics simulations. J Phys Chem C 120:9464–9474

Hoover WG (1984) Canonical dynamics: equilibrium phase-space distributions. Am Phys Soc 31:1695–1697

Humphrey W, Dalke A, Schulten K (1996) VMD: Visual molecular dynamics. J Mol Graph 14:33–38

Ilyukhina AV, Kravchenko OV, Bulychev BM (2017) Studies on microstructure of activated aluminum and its hydrogen generation properties in aluminum/water reaction. J Alloys Compd 690:321–329

Jelliss PA, Buckner SW, Chung SW, Patel A, Guliants EA, Bunker CE (2013) The use of 1,2-epoxyhexane as a passivating agent for core–shell aluminum nanoparticles with very high active aluminum content. Solid State Sci 23:8–12

Kim KT, Kim DW, Kim CK, Choi YJ (2016) A facile synthesis and efficient thermal oxidation of polytetrafluoroethylene-coated aluminum powders. Mater Lett 167:262–265

Lattin WC, Utgikar VP (2007) Transition to hydrogen economy in the United States: a 2006 status report. Int J Hydrog Energy 32:3230–3237

Liu J, Guo X (2017) ReaxFF molecular dynamics simulation of pyrolysis and combustion of pyridine. Fuel Process Technol 161:107–115

Liu H, Ye H, Zhang Y (2007) Preparation of PMMA grafted aluminum powder by surface-initiated in situ polymerization. Appl Surf Sci 253:7219–7224

Liu H, Yang F, Yang B, Zhang Q, Chaia Y, Wang N (2018a) Rapid hydrogen generation through aluminum-water reaction in alkali solution. Catal Today 318:52–58

Liu J, Liu P, Wang M (2018b) Molecular dynamics simulations of aluminum nanoparticles adsorbed by ethanol molecules using the ReaxFF reactive force field. Comput Mater Sci 151:95–105

Liu P, Liu J, Wang M (2019a) Ignition and combustion of nano-sized aluminum particles: a reactive molecular dynamics study. Combust Flame 201:276–289

Liu P, Sun R, Liu J (2019b) Adsorption behaviors of ether and aluminum surface: a molecular dynamics study. Int J Mod Phys B 33:1950028

Martínez L, Andrade R, Birgin EG, Martínez JM (2009) Packmol: a package for building initial configurations for molecular dynamics simulations. J Comput Chem 30:2157–2164

Meda L, Marra G, Galfetti L, Severini F, De Luca L (2007) Nano-aluminum as energetic material for rocket propellants. Mater Sci Eng C 27:1393–1396

Mohammadi M (2018) Exploring the possibility of GaPNTs as new materials for hydrogen storage. Chin J Phys 56:1476–1480

Mudhoo A, Torres-Mayanga PC, Forster-Carneiro T, Sivagurunathan P, Kumar G, Komilis D, Sánchez A (2018) A review of research trends in the enhancement of biomass-to-hydrogen conversion. Waste Manag 79:580–594

Nosé S (1984) A unified formulation of the constant temperature molecular dynamics methods. J Chem Phys 81:511–519

Russo MF Jr, Li R, Mench M, Duin ACT v (2011) Molecular dynamic simulation of aluminum-water reactions using the ReaxFF reactive force field. Int J Hydrog Energy 36:5828–5835

Sawamura S, Tsuchiya M, Taniguchi Y, Suzuki K (1986) Effect of pressure on the hydrogen-bond formation between phenol as a proton donor and three ethers in N-hexane. Physica B+C 139-140:732–735

Shimojo F, Ohmura S, Kalia RK, Nakano A, Vashishta P (2010) Molecular dynamics simulations of rapid hydrogen production from water using aluminum clusters as catalyzers. Phys Rev Lett 104:1–4

Shmelev V, Nikolaev V, Lee JH, Yim C (2016) Hydrogen production by reaction of aluminum with water. Int J Hydrog Energy 41:16664–16673

Stukowski A (2010) Visualization and analysis of atomistic simulation data with OVITO—the open visualization tool. Model Simul Mater Sci Eng 18:1–7

Tersoff J (1986) New empirical model for the structural properties of silicon. Phys Rev Lett 56:632–635

van Duin ACT, Bryantsev VS, Diallo MS, Goddard WA, Rahaman O, Doren DJ, Raymand D, Hermansson K (2010) Development and validation of a ReaxFF reactive force field for cu cation/water interactions and copper metal/metal oxide/metal hydroxide condensed phases. J Phys Chem A 114: 9507–9514

Wang HZ, Leung DYC, Leung MKH, Ni M (2009) A review on hydrogen production using aluminum and aluminum alloys. Renew Sust Energ Rev 13:845–853

Wang H, Feng Y, Zhang X, Lin W, Yongliang Z (2015) Study of coal hydropyrolysis and desulfurization by ReaxFF molecular dynamics simulation. Fuel 145:241–248

Wegner K, Ly HC, Weiss RJ, Pratsinis SE, Steinfeld A (2006) In situ formation and hydrolysis of Zn nanoparticles for H2 production by the 2-step ZnO/Zn water-splitting. Int J Hydrog Energy 31:55–61

Yano KH, Thomas S, Swenson MJ, Lu Y, Wharry JP (2018) TEM in situ cube-corner indentation analysis using ViBe motion detection algorithm. J Nucl Mater 502:201–212

Yoshida T, Tokumasu T (2010) Molecular dynamics study of proton transfer including Grotthus mechanism in polymer electrolyte membrane. Electrochem Soc 33:1055–1065

Zhang YR, van Duin ACT, Luo KH (2018) Investigation of ethanol oxidation over aluminum nanoparticle using ReaxFF molecular dynamics simulation. Fuel 234:94–100